

Finite Range Effects in Energies and Recombination Rates of Three Identical Bosons

P K Sørensen, D V Fedorov, A S Jensen and N T Zinner

Department of Physics and Astronomy - Aarhus University, Ny Munkegade,
bygn. 1520, DK-8000 Århus C, Denmark

Abstract. We investigate finite-range effects in systems with three identical bosons. We calculate recombination rates and bound state spectra using two different finite-range models that have been used recently to describe the physics of cold atomic gases near Feshbach resonances where the scattering length is large. The models are built on contact potentials which take into account finite range effects; one is a two-channel model and the other is an effective range expansion model implemented through the boundary condition on the three-body wave function when two of the particles are at the same point in space. We compare the results with the results of the ubiquitous single-parameter zero-range model where only the scattering length is taken into account. Both finite range models predict variations of the well-known geometric scaling factor 22.7 that arises in Efimov physics. The threshold value at negative scattering length for creation of a bound trimer moves to higher or lower values depending on the sign of the effective range compared to the location of the threshold for the single-parameter zero-range model. Large effective ranges, corresponding to narrow resonances, are needed for the reduction to have any noticeable effect.

PACS numbers: 03.65.Ge,21.45.-v,68.65.-k,67.85.-d

1. Introduction

Low-energy quantum mechanical bound states present a number of surprising results when the state contains three or more particles. The most famous case is the Efimov effect that occurs when a three-body system has two-body subsystems that have a two-body bound state with zero energy. In this situation one can mathematically prove that an infinite number of three-body states appear when the particles are bosons [1]. More generally, the effect can also take place for two-component fermionic systems whenever the mass ratios are large enough [2, 3, 4]. In recent years, it has become clear that few-body effects such as this can be studied in great detail in experiments with ultracold atomic gases via tunable Feshbach resonances [5, 6]. Producing a two-body bound state at zero energy is thus routinely done and signatures of three- and even four-body resonances have been observed [7, 8, 9, 10, 11, 12, 13, 14, 15, 16, 17].

The few-body features that are studied in ultracold atom experiments are often identified through the rate at which atoms are lost from the experimental trapping potential. In fact, the densities and lifetimes of typical Bose-Einstein-Condensates (BEC) are limited by loss effects, primarily due to three-body recombination, a process where three particles interact and create a bound system of two particles (dimer) and the third particle carries away excess energy and momentum, generally resulting in a loss of all three particles from the confining trap. The loss rate is given by $\dot{n} = -\alpha n^3$ where n is the particle density and the recombination coefficient is $\alpha = C(a)\hbar a^4/m$ with $C(a)$ a log-periodic function of the two-body scattering length a with period 22.7 [2]. A strongly interacting BEC can be created by use of Feshbach resonances where the scattering length can be tuned using an external magnetic field [6].

The a^4 scaling of the recombination coefficient is valid when the scattering length is much larger than the range of the inter-atomic potential. Here we use different models to estimate the effect of the finite range of the interactions. All the models we use are based on contact interactions but, in contrast to the typical one-parameter implementation, we also incorporate a non-zero effective range. This is done by either modifying the Bethe-Peierls boundary condition using the effective range expansion or by using a two-channel model which not only has an inherent effective range but also qualitatively describes the physics of Feshbach resonances.

The hyperspherical adiabatic approach is used to handle the three-particle problem. This method works equally well for the three scattering models we consider (zero-range contact interaction, effective range expansion and two-channel contact interaction). In order to calculate the recombination rate, we use the WKB-method with hidden crossings [18] that takes the three-body system from the initial in-coming scattering channel into the atom plus dimer channel of lower energy via an excursion into the complex plane. Since this approach depends critically on the presence of a bound dimer, it is only applicable to the positive a side of a Feshbach resonance and we only consider recombination rates for $a > 0$. Along the way, we discuss the hyperspherical potentials for the different models, and also the scaling properties of consecutive Efimov resonances when effective range corrections are included.

In order to also address the negative a side of the resonance, we calculate the spectrum of bound low-energy trimers within different models and study their dependence on the effective range corrections. Recent experiments have shown that the lowest three-body Efimov state has a breakup threshold at the three-atom continuum on the $a < 0$ side of the resonance that seems to be uniquely determined by the background van der Waals parameter of the atomic system under study [15]. In

fact, the threshold, $a^{(-)}$, is experimentally found to fulfil $a^{(-)} \sim -9.8r_{\text{vdW}}$, where r_{vdW} is the two-body van der Waals length scale [15]. This finding has induced a number of theoretical studies that aim to explain the proportionality and calculate the constant factor from basic knowledge about the two-body atomic potentials [19, 20, 22, 21, 23, 24]. It can be most easily understood as consequence of the hard-core repulsion of the atom-atom interaction (typically of Lennard-Jones type with a corresponding van der Waals tail). This fact induces a hard-core repulsion in the three-body potential around r_{vdW} as shown numerically in Ref. [21] and soon after by analytical means in Ref. [23]. Here we calculate the three-body spectrum for different scattering models and study the influence of effective range corrections on the threshold and the scaling properties of the states. Finite range corrections beyond the scattering length approximation have been considered before within various approaches [25, 26, 27, 28, 29, 30, 31, 32, 33, 34, 35]. However, to the best of our knowledge systematic studies using simple zero-range models have not been presented. Since zero-range models are extremely convenient in both few- and many-body studies, it is important to gauge their applicability which is one goal of the current study.

The paper is organized as follows: In Sec. 2 we first present the hyperspherical adiabatic method which constitutes our theoretical framework and discuss the differences in the solutions to the hyperspherical three-body potential within the different two-body interaction models that we employ. Section 3 discusses the recombination rate within the different models using the hidden crossing technique. In section 4 we discuss the spectrum of three-body bound states with the various models and map out the dependence on the effective range. Section 5 contains a short summary along with conclusions and outlook.

2. Formalism

We consider a system of three identical bosons of mass m using hyperspherical coordinates defined from the Cartesian coordinates $\mathbf{r}_i, \mathbf{r}_j, \mathbf{r}_k$, of particles i, j, k as

$$\mathbf{x}_i = \frac{\mathbf{r}_j - \mathbf{r}_k}{\sqrt{2}}, \quad \mathbf{y}_i = \sqrt{\frac{2}{3}} \left(\mathbf{r}_i - \frac{\mathbf{r}_j + \mathbf{r}_k}{2} \right), \quad (1)$$

$$\rho^2 = |\mathbf{x}_i|^2 + |\mathbf{y}_i|^2, \quad \tan \alpha_i = \frac{|\mathbf{x}_i|}{|\mathbf{y}_i|}, \quad (2)$$

where $\{i, j, k\}$ are cyclic permutations of $\{1, 2, 3\}$, ρ is the hyperradius and α_i is a hyperangle [2]. The directions of \mathbf{x}_i and \mathbf{y}_i comprise four additional hyperangles which, along with α_i , are denoted collectively as Ω . The hyperradius ρ is independent of the choice of $\{i, j, k\}$.

The wave function is expanded on adiabatic basis states $\Phi_n(\rho, \Omega)$. In the hyperspherical adiabatic approximation only the first term in this expansion is kept, this has been proven to be a good approximation when dealing with Efimov three-body states (trimers) [2]. The wave function is then

$$\Psi(\rho, \Omega) = \rho^{-5/2} f_0(\rho) \Phi_0(\rho, \Omega), \quad (3)$$

where $\Phi_0(\rho, \Omega)$ is the solution to the hyperangular equation

$$\left(\Lambda + \frac{2m\rho^2}{\hbar^2} V \right) \Phi_0(\rho, \Omega) = \lambda_0(\rho) \Phi_0(\rho, \Omega), \quad (4)$$

where Λ is the grand angular momentum operator in hyperradial coordinates (see [2]) and λ_0 is the corresponding eigenvalue. The hyperradial function $f_0(\rho)$ is a solution to the hyperradial equation

$$\left(-\frac{d^2}{d\rho^2} + \frac{\lambda_0(\rho) + 15/4}{\rho^2} - Q_{00}(\rho) - \frac{2mE}{\hbar^2}\right) f_0(\rho) = 0, \quad (5)$$

with

$$Q_{00} = \left\langle \Phi_0 \left| \frac{\partial^2}{\partial \rho^2} \right| \Phi_0 \right\rangle_{\Omega}, \quad (6)$$

where brackets indicate integration over all hyperangles. Numerically Q_{00} is found to be extremely small compared to other terms and we will not include it in further calculations. In the following we will suppress the subscript 0.

2.1. Two-body Potential Models

Our main concern is the introduction of finite range effects beyond the single-parameter zero-range approximation (where only the scattering length is included) *but* still using only contact interactions. There are different ways to do this. Here we use a boundary condition model (or range expansion model) and a two-channel model, and compare to the usual zero-range approximation with only the scattering length. To make our discussion self-contained and well-defined we now proceed to introduce first the scattering length only zero-range model and then the two effective-range models.

2.1.1. Zero-range Model. The so-called zero-range models generally use a contact interaction potential which is defined by a boundary condition on the logarithmic derivative of the wave function at zero separation. In hyperspherical coordinates this boundary condition becomes [25]

$$\left. \frac{\partial(\alpha_i \Phi)}{\partial \alpha_i} \right|_{\alpha_i=0} = -\sqrt{2}\rho \frac{1}{a_i} \alpha_i \Phi \Big|_{\alpha_i=0}, \quad (7)$$

where a_i is the scattering length between particles j and k . Since all particles are equal we will suppress indices on scattering variables such as a . Using Faddeev decomposition of the angular wave function with s -states only,

$$\Phi = \phi_1 + \phi_2 + \phi_3, \quad (8)$$

where

$$\phi_i = N(\rho) \sin\left(\nu \left[\alpha_i - \frac{\pi}{2}\right]\right) \quad (9)$$

is a solution to (4), $\nu^2 = \lambda + 4$ and $N(\rho)$ is a normalization factor, we find the eigenvalue equation

$$\frac{\nu \cos\left(\frac{\nu\pi}{2}\right) - \frac{8}{\sqrt{3}} \sin\left(\frac{\nu\pi}{6}\right)}{\sin\left(\frac{\nu\pi}{2}\right)} = \frac{\sqrt{2}\rho}{a}, \quad (10)$$

after rotating two of the Faddeev components into the coordinate system of the third [25]. For large positive ρ/a there is an asymptotic solution of the form $\nu \rightarrow i\sqrt{2}\rho/a$ yielding a dimer binding energy of

$$E_D = \frac{\lambda + \frac{15}{4}}{2\rho^2} = \frac{\nu^2 - \frac{1}{4}}{2\rho^2} \approx -\frac{1}{a^2}, \quad (11)$$

(in units where $\hbar = m = 1$). For negative a there are no bound dimers. The limit $\rho/a = 0$ yields the solution $\nu = is_0$ with $s_0 = 1.00624$. These are the basic properties of the simplest single-parameter zero-range model when applied to a system of three identical bosons.

2.1.2. Effective Range Expansion. The first method for including finite range effects beyond the scattering length is the effective range expansion (range expansion or boundary condition model for short). It is a generalization of the boundary condition (7). From scattering theory the effective range expansion of the phase shift δ as a function of wave-number k is

$$\lim_{k \rightarrow 0} k \cot \delta(k) = -\frac{1}{a} + \frac{1}{2} R k^2, \quad (12)$$

where a is the scattering length and R is known as the effective range. As it stands R is an additional parameter. However, later we will take R to dependent on the scattering length a , i.e. $R = R(a)$, since this is the physical reality of Feshbach-resonances, where both a and R are dependent on the external magnetic field (this effect arises naturally in the two-channel model described below). When we use $R(a)$ in the effective range expansion we will be assuming the same functional dependence on a as found in the two-channel model (see equation (21)) since this is a generic feature of many Feshbach resonance models [6].

The boundary condition (7) now becomes (see [25])

$$\left. \frac{\partial(\alpha_i \Phi)}{\partial \alpha_i} \right|_{\alpha_i=0} = \sqrt{2} \rho \left[-\frac{1}{a_i} + \frac{1}{2} R_i \frac{\nu^2}{2\rho^2} \right] \alpha_i \Phi \Big|_{\alpha_i=0}, \quad (13)$$

where R_i is the effective range between particles j and k , and the momentum in (12) is given by $k = \nu/(\sqrt{2}\rho)$ [25]. Again assuming that all particles are equal, the eigenvalue equation (10) becomes

$$\frac{\nu \cos\left(\frac{\nu\pi}{2}\right) - \frac{8}{\sqrt{3}} \sin\left(\frac{\nu\pi}{6}\right)}{\sin\left(\frac{\nu\pi}{2}\right)} = \sqrt{2} \rho \left[\frac{1}{a} - \frac{1}{2} R \left(\frac{\nu}{\sqrt{2}\rho} \right)^2 \right]. \quad (14)$$

Inclusion of the effective range yields the dimer binding energy

$$E_D = \frac{-1}{R^2} \left(1 - \sqrt{1 - 2\frac{R}{a}} \right)^2 \approx \frac{-1}{a^2} \left(1 + \frac{R}{a} \right), \quad (15)$$

for $|R| \ll a$. Thus the dimer system can be more or less bound depending on the sign of the effective range. In the case of atomic Feshbach resonances the effective range is negative [6], yielding less bound dimers.

This model breaks down for sufficiently large positive effective ranges since there exist no solution to the eigenvalue equation (14) for $\rho \lesssim R$ if R is positive. To remedy this deficiency an additional parameter known as the shape parameter, P , can be included in (12) [25]

$$\lim_{k \rightarrow 0} k \cot \delta(k) = -\frac{1}{a} + \frac{1}{2} R k^2 + P R^3 k^4, \quad (16)$$

and (13) gets a similar additional term. Typical values of P are around 0.1. However, we note that results from binding energy calculations are largely insensitive to the exact value of P [25]. We therefore fix $P = 0.1$ in this study. We again stress that when using (16) we take $R = R(a)$ given in (21) in order to model Feshbach resonances.

2.1.3. Two-channel Model. The other model for including finite range effects that we consider is a two-channel contact interaction model that takes the internal degrees of freedom of the atoms into account. This model has background scattering lengths in open and closed channels that we denote a_{open} and a_{closed} respectively. The full scattering length and effective range parameters of this model are (all details of this model are described in our previous work [36])

$$\frac{1}{a} = \frac{1}{a_{\text{open}}} + \frac{\beta^2}{\kappa - \frac{1}{a_{\text{closed}}}}, \quad (17)$$

$$R = \frac{-\beta^2}{\kappa \left(\kappa - \frac{1}{a_{\text{closed}}} \right)^2}, \quad (18)$$

where β parametrises the coupling between the channels and κ is given by the energy separation $E^* = \hbar^2 \kappa^2 / 2m_r$ between the channels, where $m_r = \frac{m}{2}$ is the two-body reduced mass. The expressions are valid when $a \gg \kappa^{-1}$ (equivalently $E^* \gg \hbar^2 / 2m_r a^2$), which is always the case near a Feshbach resonance. At the resonance, i.e. $a = \infty$, the effective range is [6]

$$R_0 = -\frac{1}{a_{bg}} \frac{\hbar^2}{m_r \Delta\mu \Delta B}, \quad (19)$$

where ΔB is the width of the resonance, $\Delta\mu$ the difference in magnetic moments of the channels and a_{bg} the background scattering length (the value away from the given Feshbach resonance). The resonance width ΔB and position B_0 as given in the phenomenological expression [6]

$$a(B) \approx a_{bg} \left(1 - \frac{\Delta B}{B - B_0} \right), \quad (20)$$

which can be derived in the two-channel model. The parameters a_{open} , a_{closed} , β and E^* can now be replaced by ΔB , B_0 , the difference in magnetic momenta $\Delta\mu$ and off-resonance scattering length a_{bg} to relate all quantities to physically measured values. Since we address neutral atom systems here the long-range atom-atom interaction is of the van der Waals type and can be characterized by the van der Waals length, r_{vdW} . It has been shown that the scattering length in a potential with a van der Waals tail is $\sim 0.956 r_{\text{vdW}}$ [37]. For simplicity we will assume that $a_{bg} = r_{\text{vdW}}$ and use the two interchangeably. This also means that we are working with $a_{bg} > 0$ throughout this paper. We have checked that the case with $a_{bg} < 0$ gives the same qualitative results. Off resonance the model predicts the effective range R in terms of R_0 and a

$$R(a) = R_0 \left(1 - \frac{a_{bg}}{a} \right)^2, \quad (21)$$

similar to the results obtained in [38, 39, 40, 41, 42]. Since the a -dependence of R of (21) should be generic for Feshbach resonances (independent of the particular scattering model used), we will use $R = R(a)$ in both the effective range expansion model (12) and the two-channel model.

Note that the effective range is always negative since R_0 is always negative for an atomic Feshbach resonance [6], which in turn means that the two-channel model studied here will have $R(a) < 0$ always. Multi-channel calculations of resonance

properties have shown that some Feshbach resonances can have positive R in the vicinity of the resonance (see for instance reference [10] for an example in ${}^7\text{Li}$). This is typically only found for broad resonances (with ΔB large and correspondingly small $|R_0|$). For narrow resonances with ΔB small, $|R_0|$ is large and can potentially cause non-negligible corrections to the zero-range models, this is the case we are interesting in here. Around the latter type of resonance the effective range, $R(a)$, is found to be negative. The two-channel model we employ here is only applicable to those Feshbach resonances where the effective range is negative.

2.2. Model Comparison

Before we consider the recombination rates and the binding energies in the different models, we first make a comparison of the two-body potential models in terms of their predictions for the $\nu^2 = \lambda + 4$ coefficient that provides the effective potential for the three-body system in the hyperradial equation (5). We compare the models by explicitly plotting their associated eigenvalues in figure 1. At large ρ all models have the same asymptotic value $\nu^2 = -2\rho^2/a^2$. This is because we have a two-body bound state for $a > 0$, i.e. the structure is that two particles are bound and have small interparticle distance while the third particle is far away. This is more clearly illustrated in the inset of figure 1 where the horizontal axis extends up to $\rho/a_{bg} = 1000$. For intermediate distances $\rho \gtrsim 2|R_0|$ the finite-range models show surprisingly similar forms given their quite different formalism. What is particularly important to notice is the fact that an inner pocket develops in the two-channel model, but at the same time a barrier with respect to the zero-range model is also seen. For $\rho < |R_0|$ the effective range expansion model eigenvalue goes to zero, and thus effectively becomes regularized. There is no need for a three-body parameter (in the form of a high-momentum cut-off in momentum-space or a short-distance cut-off in coordinate space). This is not the case for the two-channel model we use here. It requires a cut-off at small distance when calculating e.g. bound state energies (25) and the recombination rate (24). This can be understood by considering that the two-channel model consists of two single channel models that are coupled together by a coupling potential of zero-range. This means that there is no scale coming from the coupling that can regularize the three-body problem and in turn one still needs to introduce a short-distance cut-off as discussed in reference [36].

3. Finite-range effects in the recombination rate

We now proceed to consider three-body observables starting with the recombination rate on the positive a side of the Feshbach resonance. On this side of the resonance the recombination takes place by transition of two of the three particles into the channel with a bound two-body dimer with the universal binding energy proportional to $-a^{-2}$. On the $a < 0$ side where there is no bound dimer, the decay goes directly into some strongly bound two-body state of the atom-atom potential and depends on the short-range details. This latter case will not be considered here.

The recombination rate for $a > 0$ is calculated using the semi-classical WKB method of hidden crossing theory where the recombination coefficient α is [18]

$$\alpha = 8(2\pi)^2 3\sqrt{3} \frac{\hbar}{m_r} \lim_{k \rightarrow 0} \frac{P(k)}{k^4}, \quad (22)$$

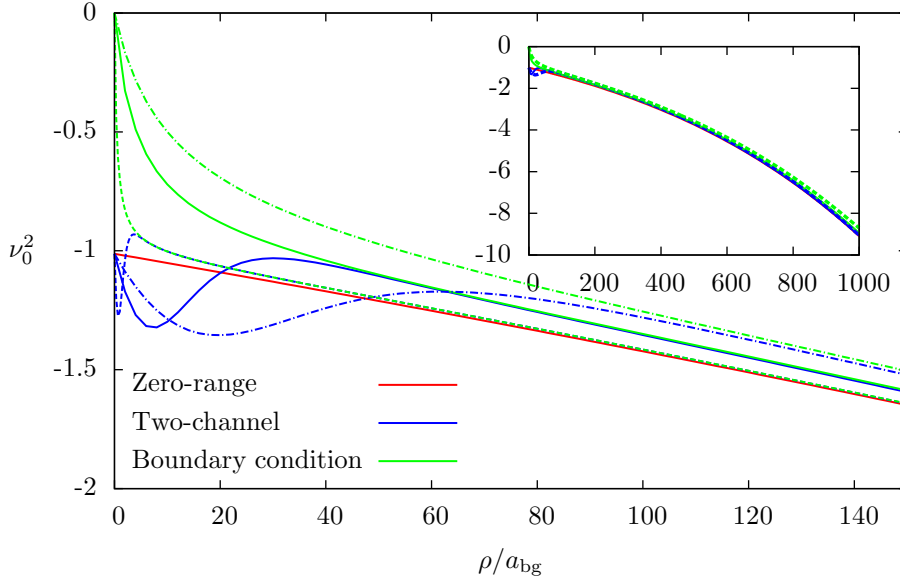


Figure 1. Small and large ρ behaviour of the hyperangular eigenvalues for $n = 0$, for the three models with $a = 500$, $R_0 = -1$ (short dash), $R_0 = -10$ (full lines) and $R_0 = -25$ (dash dot), all in units of a_{bg} .

with the wave-number k defined by $E = \hbar^2 k^2 / 2m_r$. The transition probability $P(k) \equiv |S_{01}(k)|^2$, with S_{01} the transition matrix element between adiabatic channels 0 and 1, is [18]

$$P(k) = 4e^{-2\Sigma} \sin^2 \Delta, \quad (23)$$

$$\Delta + i\Sigma = \int_{\mathcal{C}} d\rho \sqrt{k^2 - \frac{\nu(\rho)^2}{\rho^2}}, \quad (24)$$

where the integral is taken along a contour \mathcal{C} in the complex ρ -plane connecting the adiabatic channel corresponding to three free particles, $n = 1$, to the channel describing a dimer and a free particle, $n = 0$. The integration path \mathcal{C} goes around a so-called branchpoint ρ_b that connects the two channels. Additional details can be found in reference [36]. Note that since $\nu_0^2(0) < 0$ for the zero-range and two-channel models there is no classical turning point in the open ($n = 1$) channel, thus we employ a regularization cut-off in order to avoid a divergent integral.

The perhaps more familiar form $\alpha = C(a)\hbar a^4/m$ (as for instance found in reference [4]) can be found from the above equations in the universal limit ($a = \infty$) of the single channel model (where $\nu(\rho) = is_0$). Here $C(a)$ is a log-periodic function of a . We can now split the integral in two parts, one from the cutoff ρ_{cut} to the real part of the branchpoint ρ_b and another for the rest. If we denote the first part by $\Delta_1 + i\Sigma_1$, then we have the result $\Delta_1 = s_0 \log(\text{Re}(\rho_b)/\rho_{\text{cut}})$ and $\Sigma_1 = 0$. The vanishing of the imaginary part comes about since the potential is negative in the lower branch and k^2 is positive, thus yielding a purely real integrand. Now, the branchpoint is simply related to a by $\rho_b = (1.8327 + 2.1029i)a$ in the single channel model and thus $\text{Re}(\rho_b) \propto a$. When plugging this into (23) the log-periodic dependency is established.

The rest of the integration path only leads to a constant phase-shift independent of a since $\nu(\rho)$ only depends on the ratio ρ/a , see equation (10). The a^4 dependency is most easily seen by dimensional analysis, k has units of inverse length and the only available length scale in the zero range model is the scattering length a .

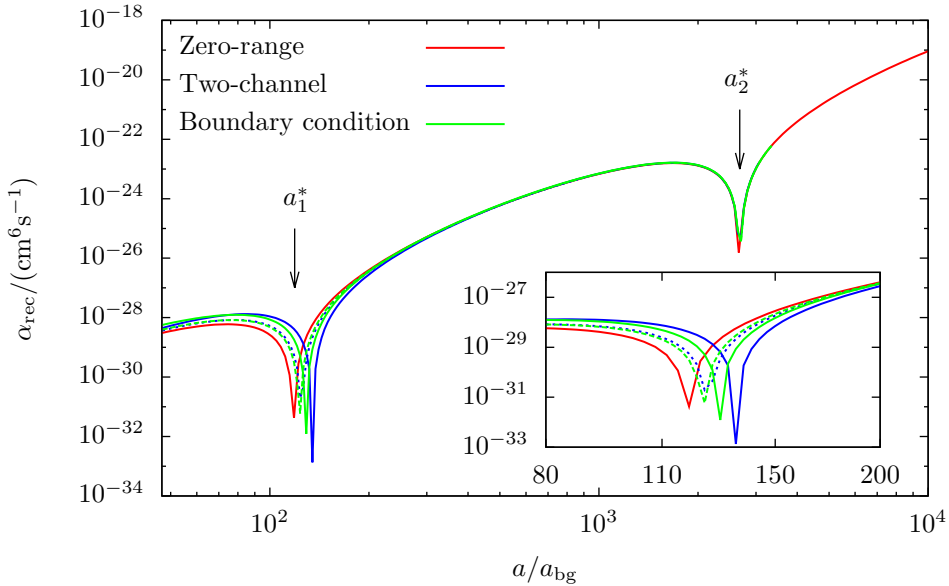


Figure 2. Recombination coefficient α (22) for the zero-range model, the effective range expansion model and the two-channel model with $R_0 = -3a_{bg}$ (dotted) and $R_0 = -10a_{bg}$ (full). The inset shows a closer look at the minimum near a_1^* . Note that the cut-off is such that all models reproduce the minimum at a_2^* . This allows us to study the effect at the other minimum of the different models.

The recombination coefficients for different values of the effective ranges and different models are shown in figure 2. The scattering length values a_1^* and a_2^* indicate locations of minima in the recombination rate. The minima are caused by the vanishing of bound trimers into the atom-dimer continuum. The cut-offs were chosen such that the minimum at a_2^* is the same for all models. We can thus compare the models at the other minimum. For the zero-range model, the ratio of a_2^* to a_1^* is 22.7, showing that this calculation scheme agrees with the universal result. For the other models this ratio is reduced, the minimum at a_1^* moves towards higher a . In order to make this more clear we plot the ratios of the minima positions as function of the effective range, R , in figure 3. We see that the two-channel and range expansion model give similar qualitative predictions but there are overall quantitative differences. We cannot extend the curves in figure 3 all the way to $R_0 = 0$ due to numerical difficulties, but the trends should be clear. What we also see is that the scale factor reduces quite drastically at large R_0 for both models. This corresponds to narrow Feshbach resonances, where there are currently not enough experimental data to make a detailed comparison.

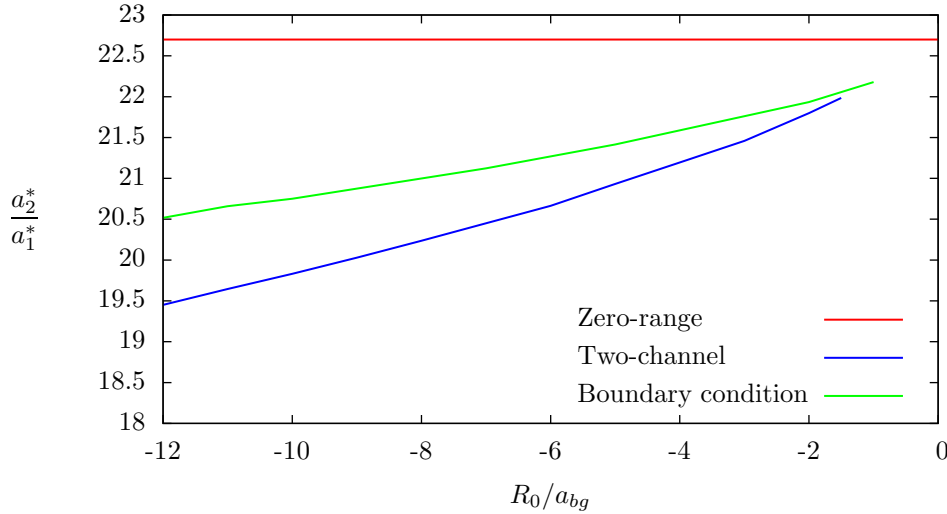


Figure 3. The ratio a_2^*/a_1^* for the zero-range model, the range expansion model and the two-channel model as function of R_0/a_{bg} . The zero-range model has a ratio of 22.7. This factor is reduced when the range is increased to more negative values.

3.1. Cut-off effects on binding energy

As we noted already above, we need to put a cut-off on the WKB integral in order to render it finite. We therefore need to consider the behaviour of the results as we change this cut-off. In particular, the choice of cut-off affects the trimer binding energy. The WKB approximation yields a simple estimate of bound state energies (similar to the Bohr-Sommerfeld quantization rule)

$$\int_{\rho_{\text{cut}}}^{\rho_t} d\rho \sqrt{2E_n - \frac{\nu_0(\rho)^2}{\rho^2}} = \pi \left(n - \frac{1}{4} \right), \quad (25)$$

where $n = 1, 2, \dots$ indicate the ground state, first excited, \dots etc. ρ_{cut} is defined at the end of Sec. 2. It is required since the potential ν_0^2/ρ^2 diverges as $\rho \rightarrow 0$ and ρ_{cut} acts as the innermost turningpoint in the WKB approximation. Likewise ρ_t is the outermost turningpoint where $2E_n = \nu_0(\rho_t)^2/\rho_t^2$.

In the universal limit $a \rightarrow \infty$ where $\nu_0(\rho) = is_0$, E_n is given by

$$E_n \approx -\frac{2s_0^2}{\rho_{\text{cut}}^2} \exp\left(-\frac{2\pi n}{s_0} + \frac{\pi}{2s_0} - 2\right), \quad (26)$$

clearly showing the geometric scaling $E_{n+1} = e^{-2\pi/s_0} E_n \approx E_n/22.7^2$ and the Thomas effect $E_n \rightarrow -\infty$ for $\rho_{\text{cut}} \rightarrow 0$.

Now we show that the cut-offs chosen such that the recombination minima at a_2^* in figure 2 coincide for the three models lead to similar trimer binding energies. Solving (25) numerically for finite scattering length gives trimer binding energies at e.g. $a = 500$, $R = -10$, $n = 2$ (in units of \hbar^2/ma_{bg}^2) which shows that the chosen cut-offs give similar bound state energies for the different models. The effect of this choice of cut-off is thus under control.

Zero-range:	$E_T = -0.002060$
Two-channel:	$E_T = -0.002441$
Effective range:	$E_T = -0.002062$

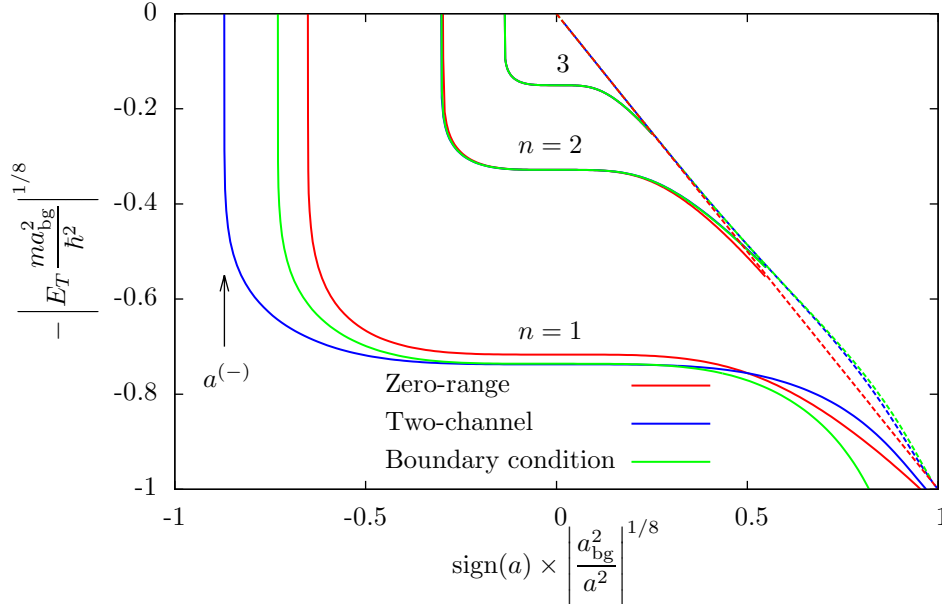


Figure 4. Trimer bound state energy E_T vs. inverse scattering length a squared for $R_0 = -5r_{\text{vdW}}$. Both axes are scaled to the power $1/8$ to reasonably fit the entire spectrum on the plot. Dashed lines indicate atom-dimer threshold.

4. Bound trimers

In order to further study the three-body physics and its dependence on two-body interaction models, we now consider the three-body bound state spectrum when finite range effects are included. When the scattering length a is large, (25) yields the same binding energy values as the radial equation (5). However, for the following discussion we will solve the radial equation numerically (5) to obtain accurate results also when the binding energy is close to zero. We solve the radial equation (5) numerically for $f(\rho)$ with the boundary condition $f(\rho_{\text{max}}) = 0$ for some large hyperradius ρ_{max} . The value of ρ_{max} is chosen such that the bound state energy has converged to the desired degree of accuracy. Also, the aforementioned cut-off ρ_{cut} is used in the boundary condition $f(\rho_{\text{cut}}) = 0$.

For the three models in question we have calculated $E(a)$ for the three lowest trimers, the result is shown in figure 4. For positive a the dashed line indicates the atom-dimer threshold which is given by the dimer binding energy $-1/a^2$ for the zero-range model and by (15) for the effective range expansion model. For the two-channel model this can be calculated only numerically, yet it agrees surprisingly well with the analytical formula for the effective range expansion model (15). The cut-offs (on the coordinate-space hyperspherical potential) were chosen such that the second trimer ($n = 2$) energies coincide at $|a| = \infty$. The three spectra for $n = 3$ are virtually identical. This is reasonable since the binding energy is very small for $n = 3$ and the

state is almost completely insensitive to finite-range effects. However, for the ground state $n = 1$ a clear distinction between the models appears. At $|a| = \infty$ the finite-range models give practically the same trimer energy, a factor of $\sim 25.3^2$ times higher than the $n = 2$ state. In comparison the zero-range model trimer energy is only a factor of 22.7^2 times higher.

We have already seen that the ratio of a -values corresponding to recombination minima in figure 2 differs from the universal value 22.7. This is directly related to the change in the atom-dimer threshold shown in figure 4 since the ratio between a corresponding to trimer energy termination points on the threshold line is no longer 22.7 for the models incorporating effective range effects.

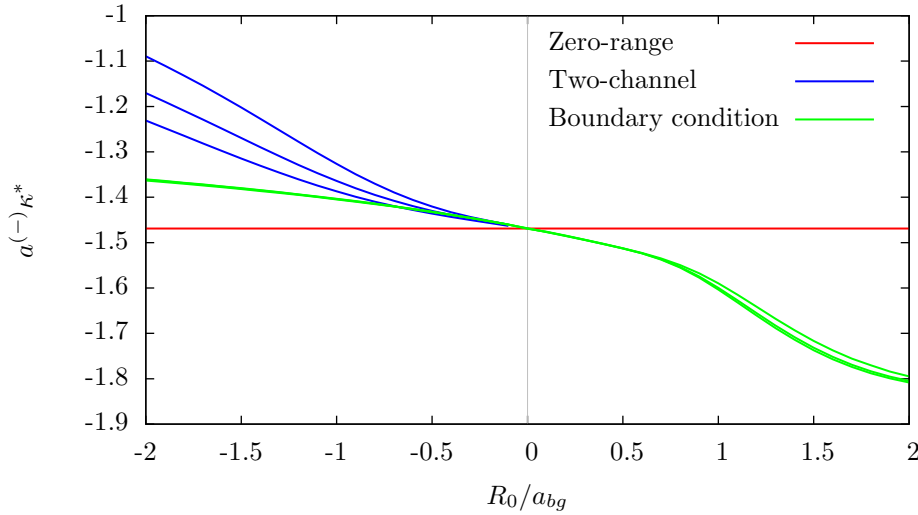


Figure 5. The product $\kappa^* a^{(-)}$ as a function of effective range, R_0 , where $-\hbar^2 \kappa^{*2}/2m_r = E_T^{(\infty)}$, $E_T^{(\infty)}$ is the trimer binding energy at resonance ($a = \infty$) and $a^{(-)}$ is the threshold scattering length for trimer creation (see figure 4). The universal value $\kappa^* a^{(-)} = -1.5076$ for the zero-range model is not correct for the lowest trimer, where the value is -1.469 , independent of cutoff. The two-channel model curves are for different value coordinate-space cut-offs on the hyperradial potential. The cut-off is 0.5, 0.6 and 0.7 in units of a_{bg} for the top, middle and bottom blue curves. For the effective range expansion model the dependency on cutoff is insignificant. Note that the two-channel model only works for $R_0 < 0$.

For negative a the value of $a^{(-)}$ indicates the threshold scattering length for creation of the lowest Efimov trimer, as indicated in figure 4. When written in units of r_{vdW} , this quantity is the subject of much recent discussion since it seems to have a universal value of $a^{(-)} \sim -9r_{\text{vdW}}$ for different cold atomic systems [15]. Here we want to address finite range effects on the value of $a^{(-)}$ for the two models. Some other recent works that address finite range effects on this threshold value can be found in reference [30] and [19].

Our results within the different models for $a^{(-)}$ as a function of R_0/a_{bg} are shown in figure 5. Most notable is the lowering of $a^{(-)}$ for the finite-range models compared to the zero-range model. This is partly due to the lower binding energy $E_T^{(\infty)}$ at $|a| = \infty$. The product $a^{(-)}\kappa^*$ (where $-\hbar^2 \kappa^{*2}/2m_r = E_T^{(\infty)}$) is universal in the zero-

range model with the value -1.5076 [43]. Thus increasing $|E_T^{(\infty)}|$ will reduce $|a^{(-)}|$. This effect is, however, not enough to account for the deviation from the zero-range result. The product is further reduced for decreasing R_0 indicating a lower value of $a^{(-)}$.

Both finite-range models show the same trend. However, the value of the change is different for the two models when $-R_0$ gets sufficiently large. The plot also shows that for the two-channel model the effect depends on cut-off. The cut-off, chosen for the purpose of illustration but with reasonable values, is 0.5, 0.6 and 0.7 for the top, middle and bottom blue curves in figure 5. The effective range expansion model shows only a very small dependence on the cut-off (the three green curves in figure 5 show very little deviation). The opposite behaviour, i.e. $|a^{(-)}\kappa^*|$ gets larger for larger effective range, is found for $R_0 > 0$. To obtain results for this case we use the boundary condition including the shape parameter (16) in the effective range expansion model in order to extend it to positive effective range. Indeed we find that the change is now opposite, see figure 5. This is similar to the product of $a^{(-)}\kappa^*$ found in reference [22]. We notice, however, that reference [22] find that the trimer binding energies for $|a| = \infty$ get smaller and the value of $|a^{(-)}|$ gets larger for large effective range. This is not seen in our calculations. This can be connected to the use of finite-range potentials with positive effective range.

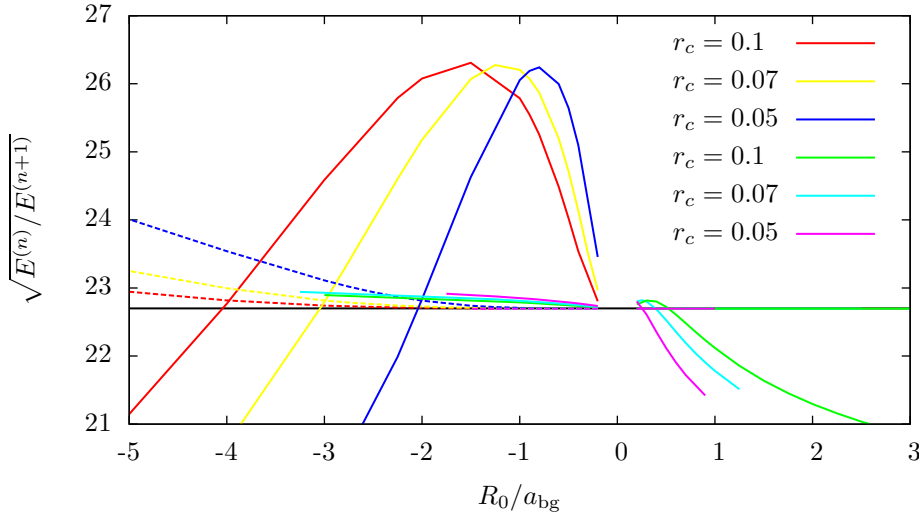


Figure 6. Ratio of trimer bound state energies at resonance as a function of effective range for several different cut-offs. The solid lines show the ratio of energies for the first and second state, the dashed lines for the second and third state. Red, yellow and blue curves (top three in legend) are for the two channel model while green, cyan and magenta curves (bottom three in legend) are for the range expansion model.

In order to better understand the behaviour of the trimer energies and $a^{(-)}$, figure 6 shows the ratio of trimer bound state energies on resonance ($|a| \rightarrow \infty$) for the two-channel and range expansion models for three different cut-offs, chosen for the purpose of illustration. The most noticeable feature is the rise and fall of the ratio of the ground state energy $E^{(1)}$ to the first excited state energy $E^{(2)}$ for the two-

channel model for negative R_0 . This non-monotonous behaviour can be understood if one assumes a three-body wave function that lives at large hyperradii, ρ . When the effective range is decreased from zero ($|R|$ increases) a barrier with respect to the pure zero-range model initially decreases the binding energy. This can be clearly seen in figure 1. As we increase the effective range further the wave function will leak into the attractive pocket at small ρ , which will again increase the binding compared to the pure zero-range result. This effect is strong for the ratio of the two lowest trimers but becomes weak for the ratio of the two highest trimers. This is understandable since the least bound trimer resides at very large hyperradii and is largely insensitive to the changes in the hyperradial potential at small ρ due to the effective range correction.

With this interpretation the behaviour can now be better understood. In figure 7 we plot the solution to (4) which determines the effective three-body hyperradial potential for the different models and for different signs of the effective range. The finite range corrections for the two-channel model and the effective range models are very different as one has the inner pocket and the other does not. This is the origin of the differences seen in figure 6. Initially we see a repulsive effect compared to the pure zero-range model that drives the ratio upwards as all states are pushed out to large distance. However, for the two-channel model we eventually feel the presence of the inner pocket and states will leak into smaller hyperradii where the ratio of energies is in turn driven down. For the positive effective range case we see from figure 7 that the range expansion model will now have a pocket at small distance. The trimer states can leak into this pocket and the ratio of energies will again go down. The important point is that in the models we have presented here there is no reason to expect monotonic behaviour since the effective three-body hyperradial potentials have non-trivial structure with repulsive and attractive parts in comparison to the pure zero-range model with no effective range corrections.

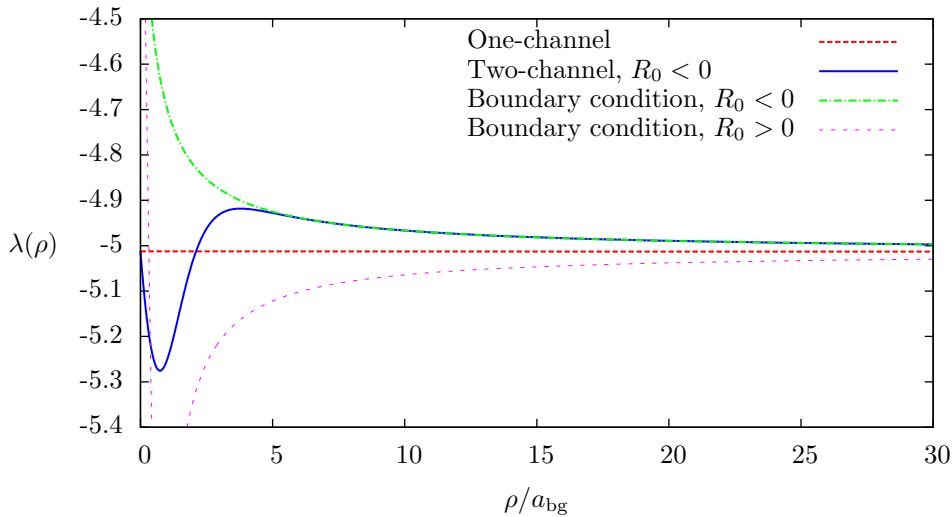


Figure 7. The eigenvalue solutions to (4) as a function of hyperradius, ρ for the zero-range, two-channel model and range expansion model for a representative case with $|R_0| = 5a_{bg}$. The lowest adiabatic potentials multiplied by ρ^2 as functions of hyperradius, ρ , for the zero range one-channel model and three different effective ranges for the two-channel model.

5. Conclusion

We investigate finite-range effects in three-body recombination rates in cold atomic gases near Feshbach resonances as well as finite-range effects in the trimer bound state energy spectrum. We use two models which include the finite-range effects and compare their results with a contact interaction (i.e. zero-range) model. The first model is the range expansion model which is a straightforward extension of the zero-range contact interaction model. Here the effective range is included directly in the boundary condition on the three-body wave function following the effective range expansion of standard scattering theory. Variation of the scattering length through the Feshbach resonance is done phenomenologically as in the zero-range model. This model can also be used for positive effective range calculations. The second model is a two-channel contact interaction model which naturally includes both the finite effective range and the variation of the scattering length through the Feshbach resonance.

We show that with these well-tested two-body interaction models the three-body physics can display complicated non-monotonic behaviour as the effective range is varied. In particular, we find that the geometric scaling factor of 22.7 for equal mass particles changes when including range corrections, and that it can become both larger and smaller than 22.7 depending on the magnitude and sign of the effective range.

In the current setup this can be understood based on the functional form of the effective hyperradial potential. On resonance where the scattering length diverges, the lowest trimer bound state has the strongest dependency on effective range since it lives at small hyperradius, whereas the excited states live at much larger hyperradii and the effective range contribution is much less pronounced. The adiabatic potential of the range expansion model is raised and lowered relative to the zero-range model potentials when the effective range is negative and positive, respectively. This leads to bound states being less or more bound, respectively. For the two-channel model the effective range is always negative which can only be achieved by using potentials with an outer barrier. The hyperradial potential reflects this fact and develops a pocket at small hyperradii that the lowest states will eventually leak into. This feature is similar to the range expansion model *but* for the case of positive effective range.

Our results demonstrate that effective range corrections within the framework of contact model potentials can lead to non-trivial behaviour of trimer energies, thresholds and interference features in recombination rates. Effective range corrections are expected to be important for the case of narrow Feshbach resonances. The experimental data on Efimov states for narrow resonance systems is sparse and more measurements are needed in order to fully discriminate between different models that include finite range corrections. However, what we can conclude is that care must be taken when a particular two-body scattering model is used for the trimer states that have the largest binding energies in a universal setup, i.e. for the lowest states that have binding energies related to the background short-range scales. For higher lying trimers it is less important since the states are largely insensitive to the short-distance behaviour of the effective three-body potential.

Acknowledgements This work was supported by the Danish Agency for Science, Technology, and Innovation under the Danish Council for Independent Research - Natural Sciences.

References

- [1] Efimov V *Yad. Fiz* 1970 **12** 1080; Efimov V 1971 *Sov. J. Nucl. Phys.* **12** 589
- [2] Nielsen E, Fedorov D V, Jensen A S and Garrido E 2001 *Physics Reports* **347** 373
- [3] Jensen A S, Riisager K, Fedorov D V and Garrido E 2004 *Rev. Mod. Phys.* **76** 215
- [4] Braaten E and Hammer H-W 2006 *Phys. Rep.* **428** 259
- [5] Ferlaino F and Grimm R 2010 *Physics* **3** 9
- [6] Chin C, Grimm R, Julienne P S and Tiesinga E 2010 *Rev. Mod. Phys.* **82** 1225
- [7] Kraemer T *et al* 2006 *Nature* **440** 315
- [8] Pollack S E, Dries D and Hulet R G 2009 *Science* **326** 1683
- [9] Zaccanti M *et al* 2009 *Nature Phys.* **5** 586
- [10] Gross N, Shotan Z, Kokkelmans S and Khaykovich L 2009 *Phys. Rev. Lett.* **103** 163202
- [11] Williams J R, Hazlett E L, Huckans J H, Stites R W, Zhang Y and O'Hara K M 2009 *Phys. Rev. Lett.* **103** 130404
- [12] Gross N, Shotan Z, Kokkelmans S and Khaykovich L 2010 *Phys. Rev. Lett.* **105** 103203
- [13] Lompe T, Ottenstein T B, Serwane F, Wenz A N, Zürn G and Jochim S 2010 *Science* **330** 940
- [14] Nakajima S, Horikoshi M, Mukaiyama T, Naidon P and Ueda M 2011 *Phys. Rev. Lett.* **106** 143201
- [15] Berninger M *et al* 2011 *Phys. Rev. Lett.* **107** 120401
- [16] Wild R J *et al* 2012 *Phys. Rev. Lett.* **108** 145305
- [17] Knoop S, Borbely J S, Vassen W and Kokkelmans S J J M F 2012 *Phys. Rev. A* **86** 062705
- [18] Nielsen E and Macek J H 1999 *Phys. Rev. Lett.* **83** 1566
- [19] Naidon P, Hiyama E and Ueda M 2012 *Phys. Rev. A* **86** 012502
- [20] Chin C 2011 arXiv:1111.1484v2.
- [21] Wang J, D'Incao J P, Esry B D and Greene C H 2012 *Phys. Rev. Lett.* **108** 263001
- [22] Schmidt R, Nath S P and Zwerger W 2012 *Eur. Phys. J. B* **85** 386
- [23] Sørensen P K, Fedorov D V, Jensen A S and Zinner N T 2012 *Phys. Rev. A* **86** 052516
- [24] Naidon P, Endo S and Ueda M 2012 arXiv:1208.3912.
- [25] Fedorov D V and Jensen A S 2001 *J. Phys. A: Math. Gen.* **34** 6003
- [26] Kokkelmans S J J M F, Milstein J N, Chiofalo M L, Walser R and Holland M J 2002 *Phys. Rev. A* **65** 053617
- [27] Fedorov D V and Jensen A S 2002 *Few-Body Syst.* **31** 229
- [28] Jonsell S 2004 *J. Phys. B: At. Mol. Opt. Phys.* **37** S245
- [29] Petrov D S 2004 *Phys. Rev. Lett.* **93** 143201
- [30] Thøgersen M, Fedorov D V and Jensen A S 2008 *Phys. Rev. A* **78** 020501(R)
- [31] Platter L, Ji C and Phillips D R 2009 *Phys. Rev. A* **79** 022702
- [32] Thøgersen M, Fedorov D V, Jensen A S, Esry, B D and Wang Y 2009 *Phys. Rev. A* **80** 013608
- [33] Ji C, Phillips D R and Platter L 2010 *Europhys. Lett.* **92** 13003
- [34] Wang Y, D'Incao J P and Esry B D 2011 *Phys. Rev. A* **83** 042710
- [35] Zinner N T 2011 arXiv:1112.6358
- [36] Sørensen P, Fedorov D V and Jensen A S 2012 *Few Body Systems* Online first arXiv:1112.4962
- [37] Gribakin G F and Flambaum V V 1993 *Phys. Rev. A* **48** 546
- [38] Gao B 1998 *Phys. Rev. A* **58** 4222
- [39] Flambaum V V, Gribakin G F and Harabati C 1999 *Phys. Rev. A* **59** 1998
- [40] Zinner N T and Thøgersen M 2009 *Phys. Rev. A* **80** 023607
- [41] Thøgersen M, Zinner N T and Jensen A S 2009 *Phys. Rev. A* **80** 043625
- [42] Zinner N T 2012 arXiv:0909.1314
- [43] Gogolin A O, Mora C and Egger R 2008 *Phys. Rev. Lett.* **100** 140404